THE MICHIGAN STATE UNIVERSITY SUPERCONDUCTING CYCLOTRON PROGRAM*

H. G. Blosser

Cyclotron Laboratory, Michigan State University
East Lansing, Michigan 48824

Summary

Status of the superconducting cyclotron program is reviewed as of September 1978. A number of design details have changed since the previous conference. Novel features have been checked in a variety of prototype test facilities.

Text

In June 1975 the MSU Cyclotron Laboratory received authorization to proceed with construction of a full scale prototype magnet for a 500 MeV superconducting cyclotron. The objective of this program was to establish basic feasibility of accelerator systems using such magnets. In May 1977 operating tests of the protoptype magnet were started; first operation at full design current occurred on May 26, 1977. Overall performance of the prototype magnet was excellent and in August 1977 the laboratory received authorization to proceed with a so called "Phase I" accelerator program, namely, a program to make the 500 MeV magnet into a working cyclotron and to connect this cyclotron with existing experimental facilities. This Phase I program is very much in mid-stream at present. First operating tests of the cyclotron are expected in the Fall of 1979 and nuclear physics use is expected to begin early in 1980. The laboratory has also submitted a proposal for a further major expansion, namely adding a second 800 MeV superconducting cyclotron as a booster for the 500 MeV machine and including additions to the laboratory building and to experimental facilities which would approximately double the size of the present installation. The proposal has received a high priority recommendation for funding in fiscal year 1980. If this proceeds as planned the full two cyclotron system is expected to come into use in early 1984.

Many of the subsystems of this overall project are described in specific topical papers appearing elsewhere in these proceedings i.e., central region, rf system, cryogenic system, magnetic field studies, trimming optimization studies, extraction studies, injection studies for the second stage, and overall design of the K800 cyclotron. The objective of this summary paper is to convey a somewhat more casual and largely pictorial glimpse of the actual status of the project as of September, 1978.

The core of the presentation is in the following six pages which present Figures 1 through 23. These figures and the technical comments included with the captions show a number of construction details of the K500 cyclotron and performance expected from the system. The figures also show a number of prototype assemblies built to test various features of the design.

In reviewing the figures, a number of major design changes can be seen relative to descriptions given at the 1975 cyclotron conference reflecting evolution of design concepts as the program evolved as well as adaptations to unexpected results from some protopype tests. The idea of using an inert superconducting extraction channel has been laid aside, for example, following a series of prototype tests of these so called "super-tubes", which gave a mixture of good and bad results and a sense of inadequate reliability of such elements as a key subsystem of a major accelerator project. The presently envisaged extraction system then consists of electrostatic deflectors which operate well within established technical limits on electric fields. The electrostatic deflectors are supplemented by sets of inert iron focusing bars positioned in a pattern which gives a field combining a strong quadrupole and a weak dipole component. The overall combination of deflector and focusing bars gives a very attractive extraction trajectory with excellent optical characteristics.

A major change in the rf system relative to the 1975 design is a lowering of the frequency range by an approximate factor of 3 and a correlated decision to make extensive use of harmonic numbers 1, 2, 4, etc., which require phasing of the dees by multiples of 120°. Phasing of 120° is a feature not previously used in cyclotrons except for a brief early test at Berkeley and a rather realistic model was therefore built to check tuning characteristics of a system of this kind. Orbit properties of the overall system are much improved by having the rf frequency more nearly match the orbital frequency and an overall sizeable improvement in beam quality is expected from the lower frequency system.

The lower frequency range involves dee stems of rather awkward length--at 9 Mhz the sliding short is ∿ 16' from the median plane--estimates of mechanical vibrations in dee stems of this length indicated serious problems for 4" diameter unsupported stems. Dee stem insulators have therefore been introduced just below the magnet yoke. These also then form a boundary for the vacuum envelope and allow the sliding shorts which tune the dees to operate in air.

The vacuum system for the cyclotron is a somewhat complicated three part chamber, namely a completely separate all metal enclosure as the insulating jacket for the main coil, secondly, a high quality cryopumped metal gasketed chamber for the beam space and thirdly, a low quality "coil" vacuum contained between the pole caps and the copper rf liners enclosing both pole tips and pole tip correction windings.

*Work supported by the U.S. National Science Foundation Grant #s 75-01080, PHY76-83254, and PHY78-01684.

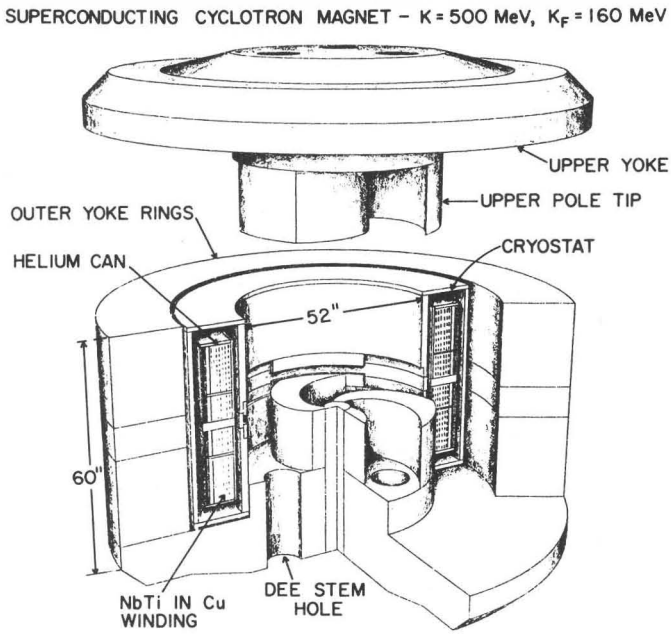

Figure 1. Conceptual drawing of the K500 magnet showing major elements of the coil, yoke, and pole tip system. The upper pole cap is in the raised position. The cryostat wall is constructed of mild steel except for a non-magnetic median plane insert.

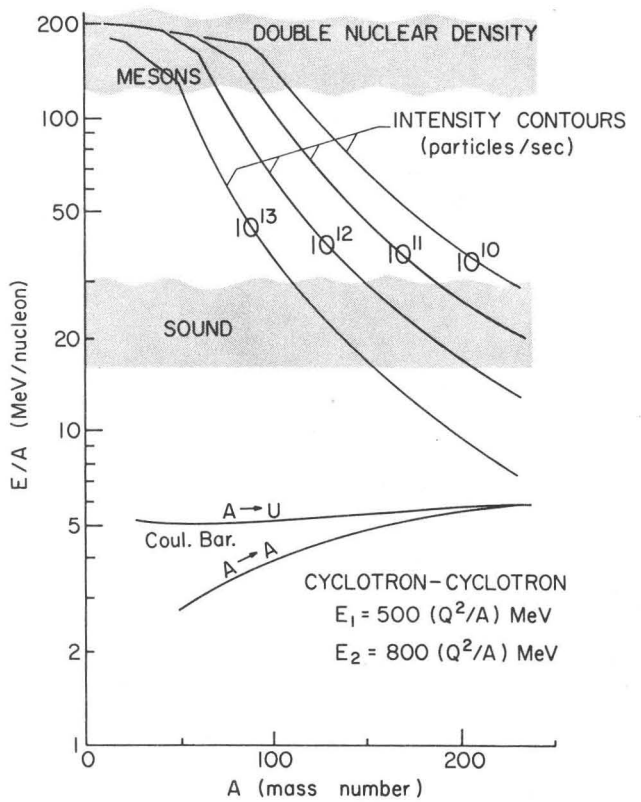

Figure 2. Approximate smoothed intensity contours for coupled K500 and K800 cyclotrons. The gray bands show the overlap between the operating range and theoretical estimates of the onset of nuclear compressional waves, coherent mesic phenomena and doubling of the nuclear density. (More accurate performance estimates based on detailed calculation of the K800 are given in the paper by Resmini.)

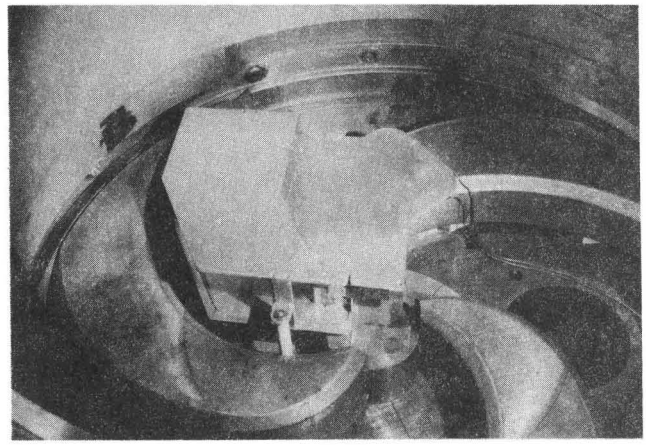

Figure 3. Photograph of lower pole tip with ion source testing charge collector mounted in position. (The charge collector operates at DC bias of 30 kV and is equipped with a multi-wire collecting grid for study of charge state distributions.)

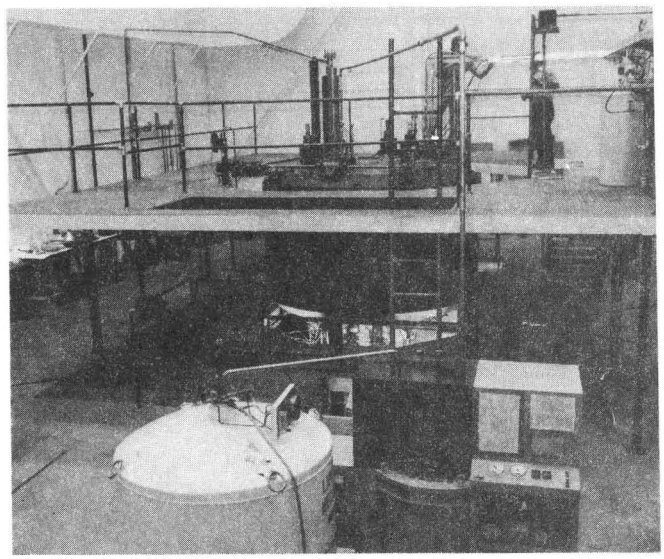

Figure 4. View of the helium refrigerator and liquid storage tank with the K500 magnet in the background.

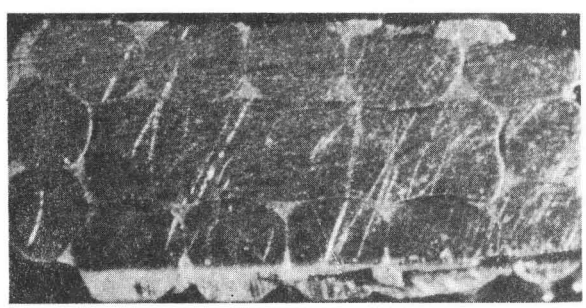

Figure 5. Conductor magnified 15x. Niobium-titanium filaments are embedded in three 40 mil diameter copper wires located at the left and at the upper and lower right in the photo. (Each bundle contains 115 filaments, each 2 mils in diameter.) The three superconducting bundles are spirally wrapped along with ten pure copper wires around a rectangular copper core and bonded with soft solder to form an overall 0.110" by 0.196" conductor.

0018-9499/79/0400-2041$00.75 ©1979 IEEE

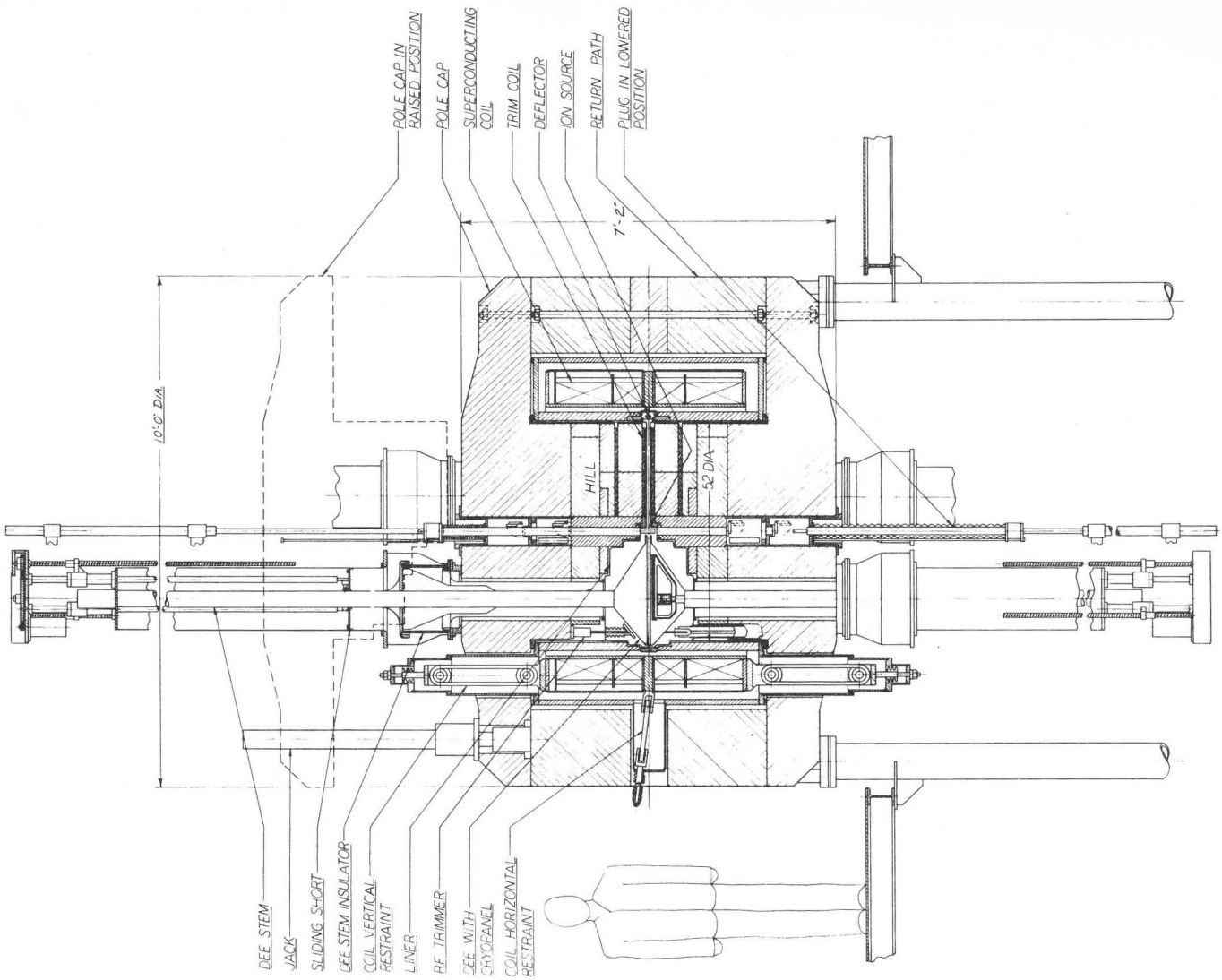

Figure 6. (right) Vertical section view of the K500 cyclotron. (In the pole tip region the section view is along a line of constant spiral.) The coil is held in position by a set of nine support links (3 up, 3 down, 3 radial) constructed of epoxy and fiber-glass laminate. The lower half of each dee contains a cryo-panel which directly views the beam space. The rf drive line feeds through a cup shaped variable capacitor which can be seen at the outer edge of the lower part of the dee. Identical non-magnetic ion sources enter from top and bottom vacuum locks at the cyclotron center, so that cathode changes and source pump-out can be performed while the cyclotron is running on the other source.

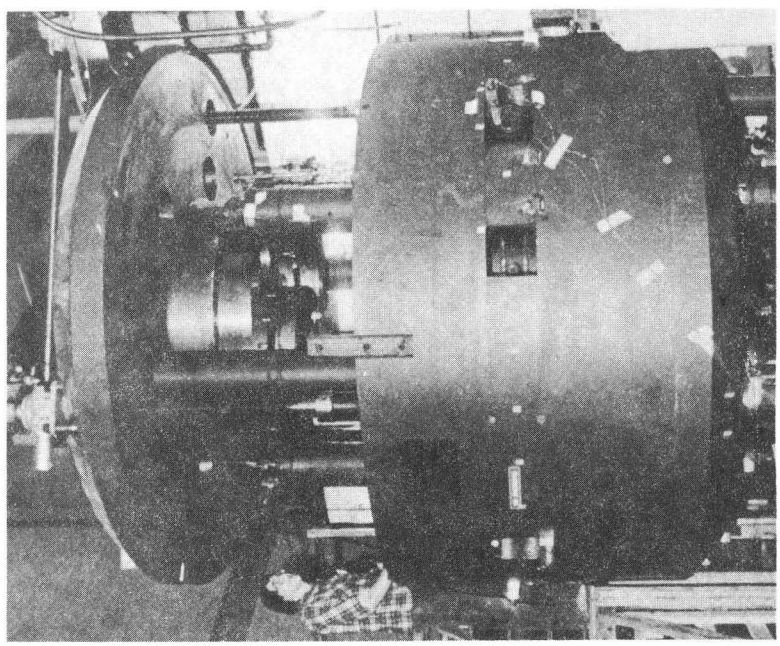

Figure 7. Photograph of the K500 magnet with top raised for access. The upper set of pole tips can be seen near the center.

0018-9499/79/0400-2042$00.75

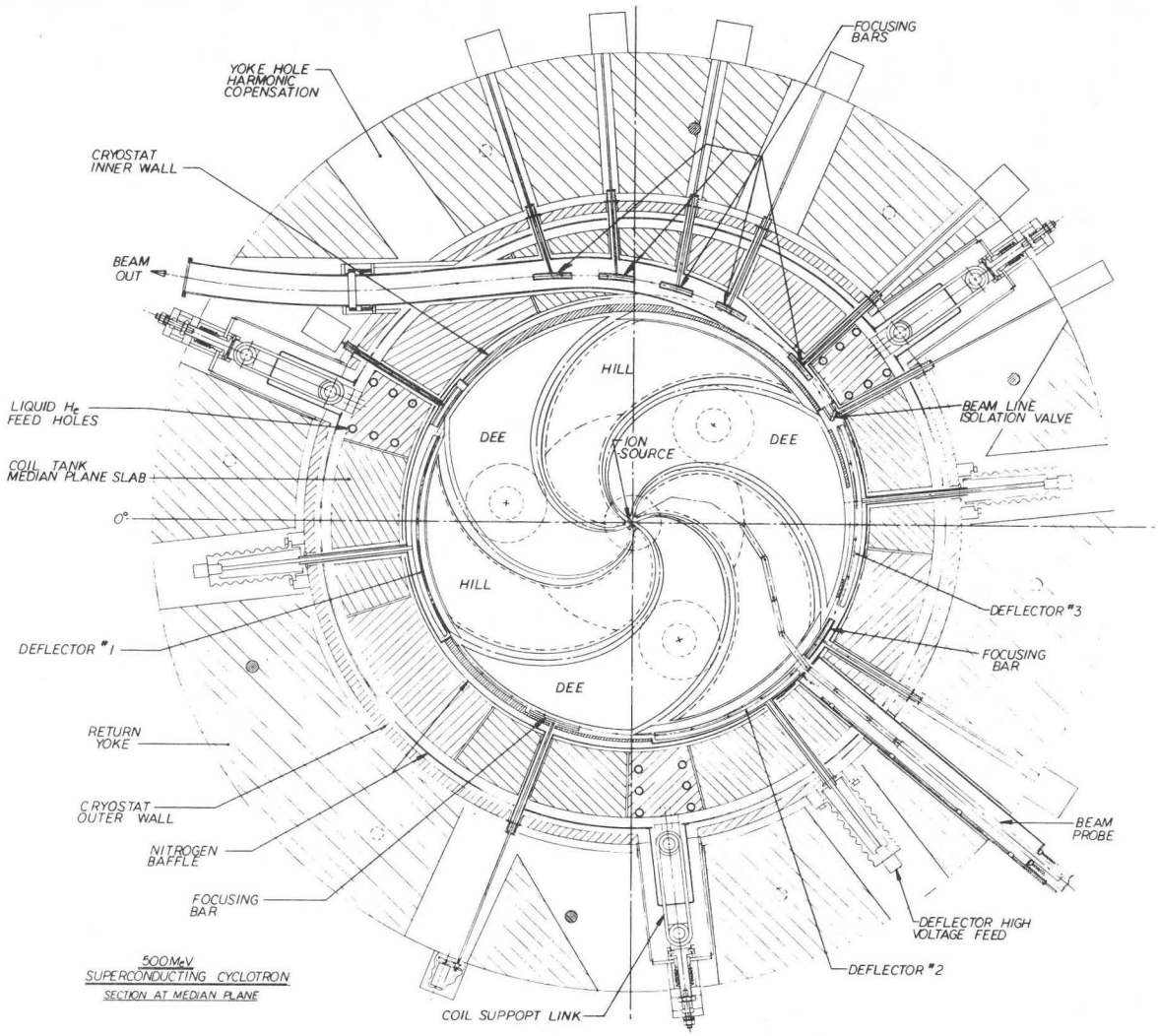

Figure 8. Median plane view of the K500 cyclotron. Dashed lines mark the edge of the pole tip steel and the dee stem and dee stem housing. The dot-dashed lines show the design angular location of the acccelerating gaps ($\tau = r/13" + n\times\pi/3$). The helium bath for the upper and lower sections of the main coil connects only through the 18 "liquid helium feed holes." The remainder of the median plane periphery of the coil is composed of stainless steel slabs which can be removed for installation of median plane penetrations (extraction elements, probes, etc.).

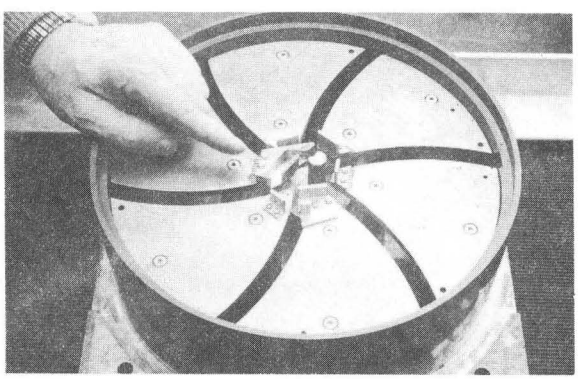

Figure 9. Photo of three dimensional one-to-one scale electrolyte tank. The lip of the tank wall (and the surface of the central electrodes) marks the median plane. The source position and other central region structures are set for first harmonic operation.

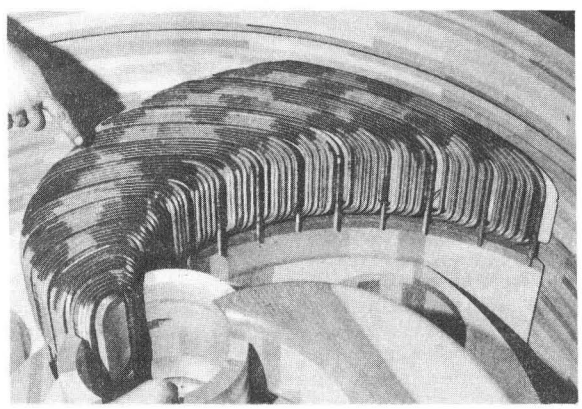

Figure 10. Prototype set of trim coils mounted on the full scale wooden model. The dark line on the outer periphery marks the median plane. Each of the thirteen coils has nine and one half turns of 0.25" x 0.25" hollow copper conductor.

0018-9499/79/0400-2043$00.75 ©1979 IEEE

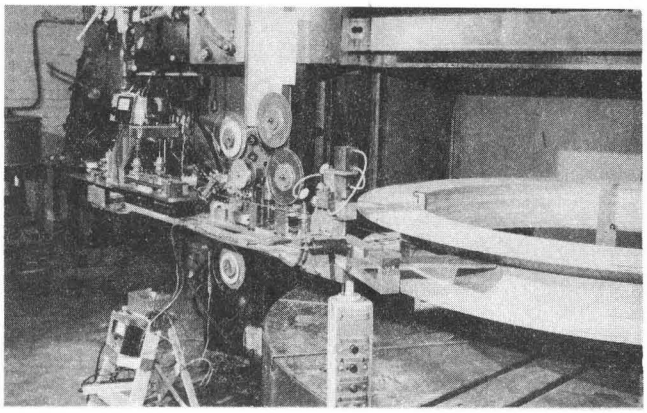

Figure 11. Photograph of the coil winding machine set up for practice winding. Mylar insulation (stored on the circular reels) was creased and applied to the conductor directly in the winding line in a fashion which left the conductor surface 50% bare. The winding line also includes an accurate tensioning system (with the capability of maintaining tensioning during possible unwinding cycles), a presser foot to pack each turn of conductor tightly against its neighbor, a dimension checking circuit to monitor the conductor for possible protruding filaments and a feed mechanism which advances the whole winding apparatus helically along the coil.

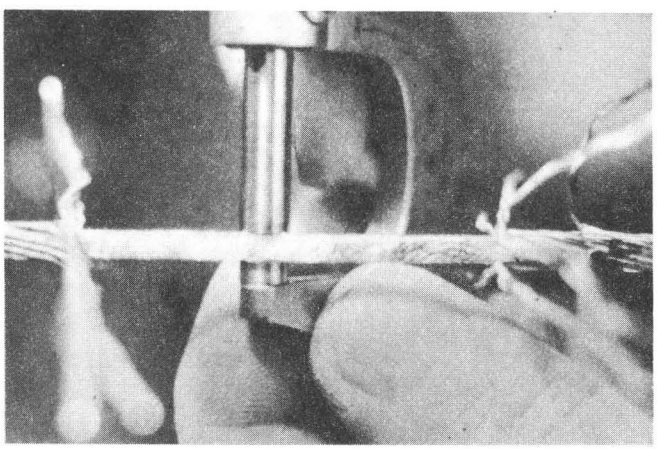

Figure 12. Photograph of conductor in the process of splicing. The central copper core has been joined in a scarf type hard solder joint. The conductor filaments will next be rebraided in rope-like fashion and soft soldered (13 of the copper strands being clipped at staggered points). The coil contains 15 such splices. Acceptable splices did not exceed the linear dimension of the unspliced conductor by more than 10 mils. A resistance measurement on a test splice gave 1.4×10^{-9} ohms at 4.2° and 5 tesla. Pull tests on 5 samples gave values greater than 90% of the breaking strength of unspliced conductor.

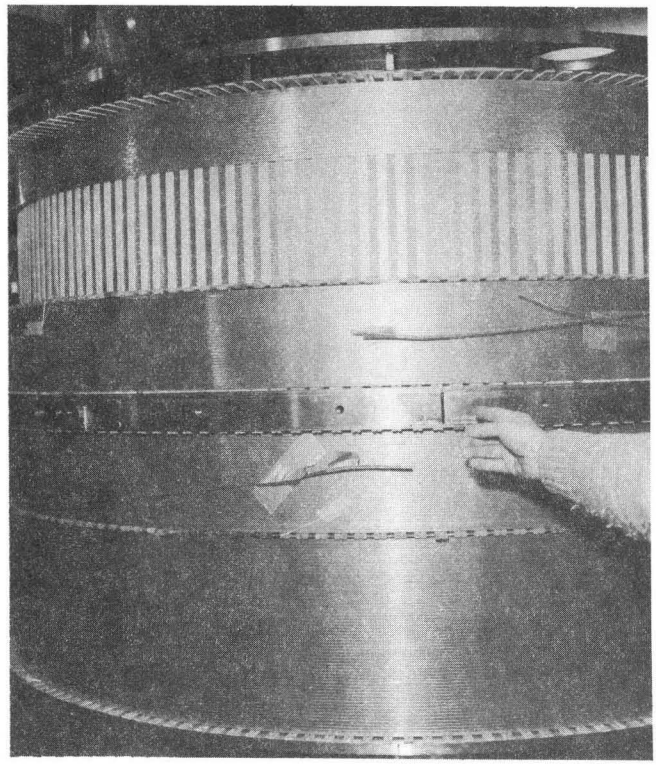

Figure 13. Photograph of the coil near the end of the winding cycle. The hand touches one of the removable stainless steel median plane slabs. Winding of the two small coil sections near the median plane and of the lower large section is completed, and winding of the upper large coil section is nearing completion. The vertical "picket fence" across the upper center is a layer of 40 mil thick G-10 strips inserted between conductor layers, the regions between the strips forming channels for liquid helium. At the point when the photograph was taken, a coil layer is approximately 30% finished and feeding on downward from the left. This will continue over the region where the pickets are exposed after which another layer of pickets will be inserted and winding of a reverse upward layer will begin.

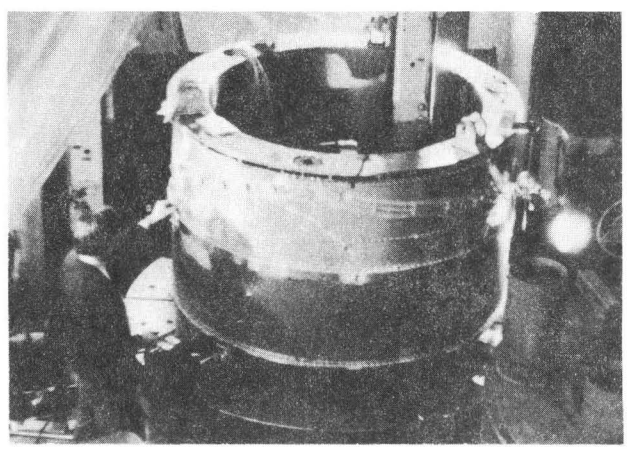

Figure 14. Final view of the superconducting coil just before welding on outer stainless steel wall to seal the helium can. The coil leads form a tracklike pattern on the outer surface. A final test for grounds is being performed.

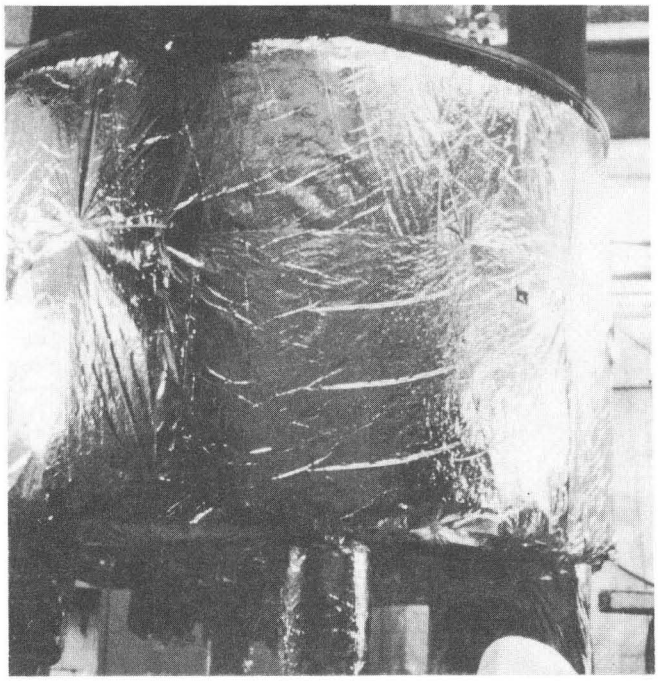

Figure 15. Photo of the coil after installation of aluminized mylar superinsulation.

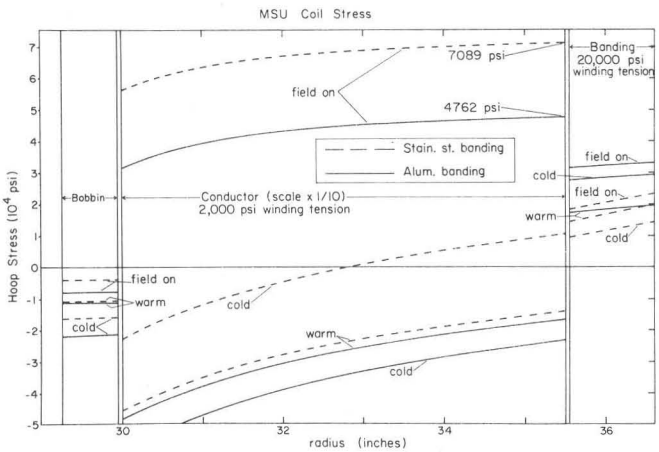

Figure 16. Calculation of internal stress in the coil assuming outer banding of stainless steel (dashed curves) and of aluminum (solid curves). The curves labeled "warm" give the stress distribution at the time winding is completed i.e., with the coil under compression due to the high winding tension in the outer banding and the bobbin under compression due to the winding tension of both coil and banding.(Note that stress curves for the coil are expanded ten fold relative to bobbin and banding.) Cooling the coil causes a redistribution of tensions due to differing thermal contractions of the several materials. Turning on the field gives a second redistribution of stresses as a result of the magnetic force on the conductor. Based on these calculations, aluminum banding was selected because it leads to a lower final stress in the conductor as a result of the greater contraction of the banding in the cooling process. Note that even though the"field on"condition leads to a positive stress in the conductor, the bobbin remains under compression indicating that the coil is still pressing in on the bobbin. No position shift of the coil relative to the bobbin should then occur.

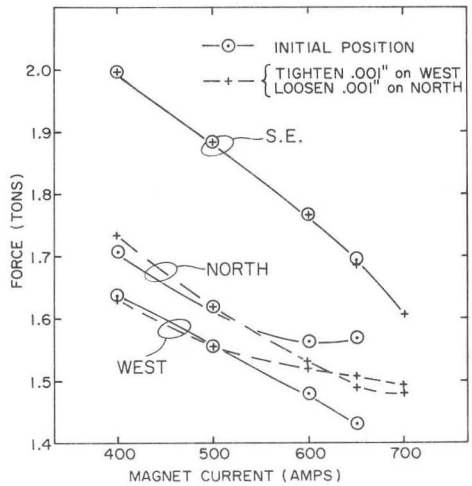

Figure 17. Experimental data from strain bolts in the three radial support links vs. magnet current. The run labeled "Initial Position" was terminated at 650 amps because the tension in the north link had ceased to decrease. The extreme sensitivity of the system is indicated by the second run in which a one mil change in the relative West/North position gives a large shift in the relative behavior of the two forces.

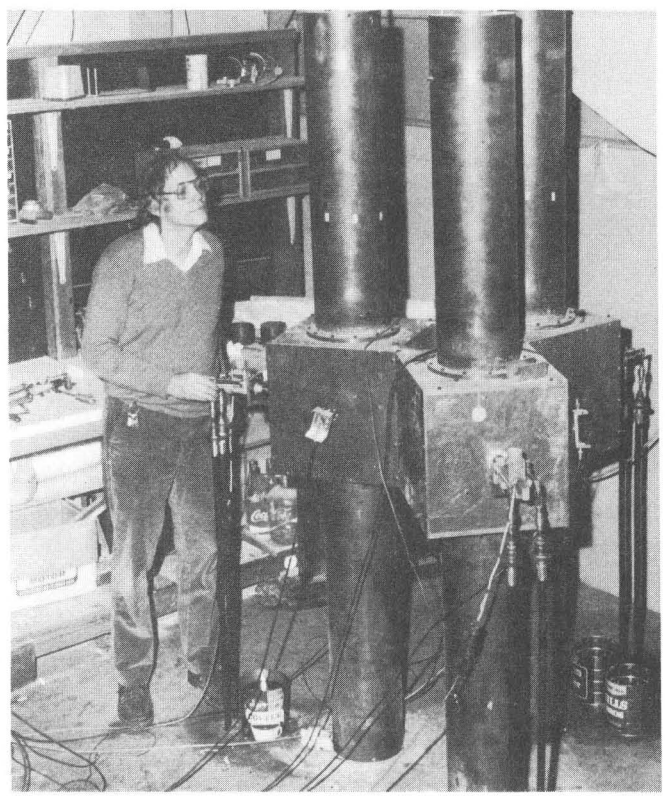

Figure 18. Photograph of high "Q" tuning model. Dees and dee-to-dee coupling are included as lumped elements. Dee stems, tuning servoes, and drive circuits correspond to actual structures which would be used in the completed cyclotron. Servo circuits were developed which accurately regulate the phase difference between dees to any desired multiple of 120°. Measured "Q" of the model is 6000.

0018-9499/79/0400-2045$00.75 ©1979 IEEE

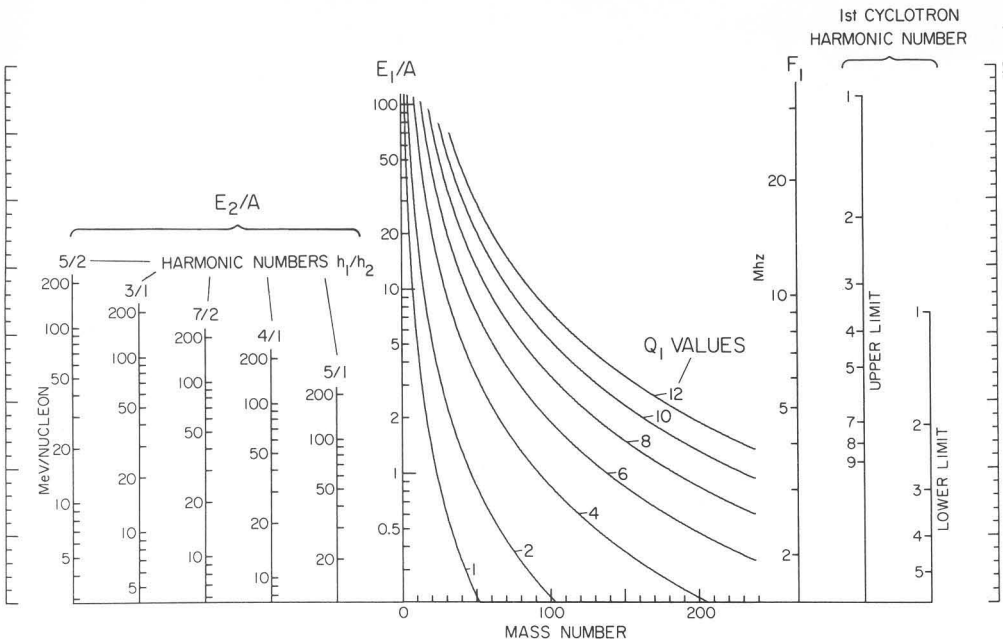

Figure 19. Energy multiplication and frequency plot when the first cyclotron is operating at peak field. A horizontal line reads out the orbital frequency in the first cyclotron, limiting energy for various values of the charge in the first cyclotron, and the energy from the second cyclotron for various values of the harmonic ratio. The two right hand columns give upper and lower frequency limits for various harmonics assuming the RF operates in the range 9 to 32 Mhz.

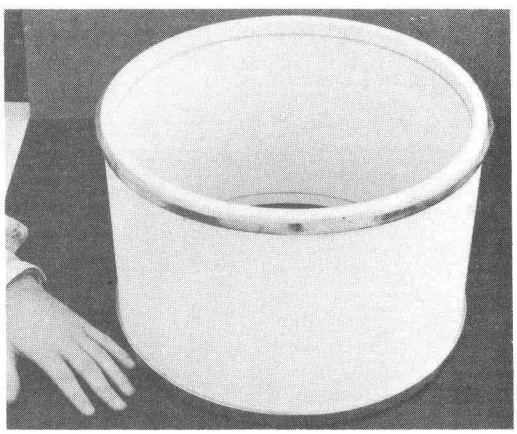

Figure 20. Photo of dee stem insulator fabricated from 99.5% alumina 10" high x 16" in diameter with 0.375" thick walls and with vacuum tight copper rings brazed at top and bottom for attachment to main vacuum wall.

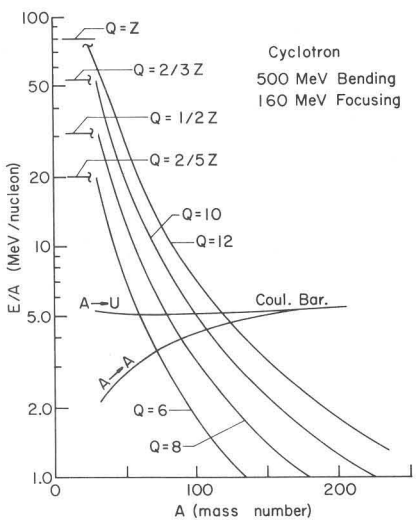

Figure 21. Energy per nucleon vs mass number for ions of various charge assuming the K500 is operating as a stand alone cyclotron.

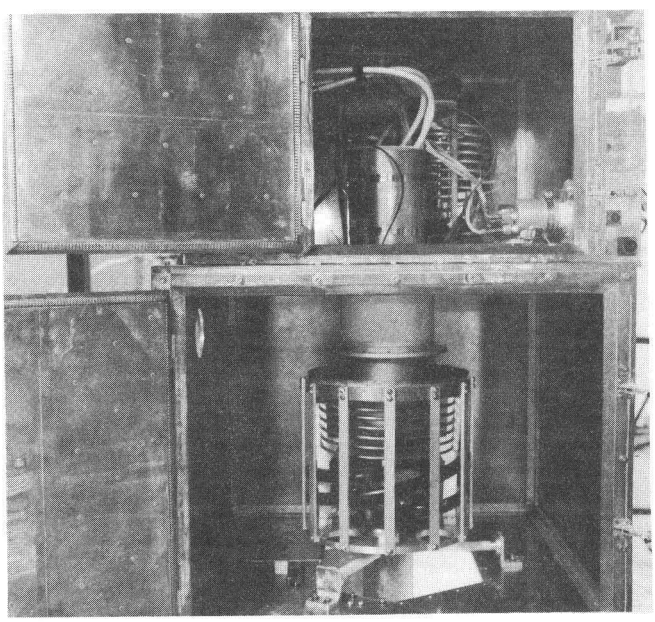

Figure 22. View of prototype RF amplifier. The grid box is at the top, the plate box at the bottom. The plate structure of the 4CW100,000 is visable just below the separating partition.

0018-9499/79/0400-2046$00.75 ©1979 IEEE

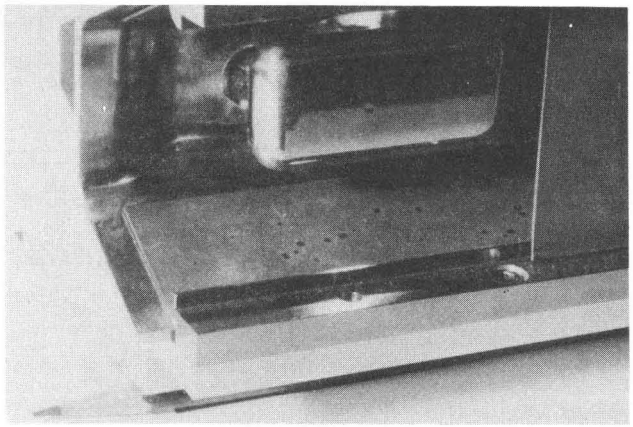

Figure 23. Photograph of deflector test assembly. Electrode cross section, clearances and insulators have the same dimensions as planned K500 deflectors. Tests in the 1.8 tesla magnetic field of the K50 cyclotron baked in easily to the power supply limit (electric field of 140 kV/cm).

** DISCUSSION **

J. REICH: Is it possible to axially inject highly stripped ions from ion sources, such as those to be discussed.

H. BLOSSER: Resmini has looked briefly at axial injection, making a scaling comparison relative to the LBL 88" cyclotron system. It seems from this that an axial injection system could readily be designed, but no detailed work is in progress. The magnet, of course, has an easily removable central plug.

Y. JONGEN: Why did you discard the supertube extraction method?

H. BLOSSER: The first supertube which we tested had an unexpectedly low shielding capability of about 4 kG – about one-tenth that expected. The second tube tested well, but in the meantime an electrostatic system had been calculated: we feel it offers comparable performance with a more established technology. An important factor in the electrostatic system is the addition of inert ion "focusing bars," as suggested by C. Hoffman of Chalk River.

T. KUO: Would you tell us how to take the beam through the cryogenic enclosure of the superconducting magnet?

H. BLOSSER: The coil has a 2" thick removable stainless steel slab in the median plane. There are about a dozen penetrations through cut-outs in this slab, half of which are already installed, half of which will be installed next spring. Heat leaks from these penetrations are small.

J. MARTIN: The drawing identifying the various regions of different magnetization used in the TRIM calculation showed M=0 regions in the yoke on the midplane and in the yoke just above the coil space. Please explain what the M=0 regions represent.

H. BLOSSER: The code we use (TRIM – Colonias – LBL) allows only a limited number of different magnetization values. The number of distinct M regions in the magnet exceeds the number allowed by the code. For those far away from the beam, we then substitute a weighted mixture of M=0 and M=1 to represent the proper iron fraction.

W. JOHO: Do you have enough clearance on the first orbit in the center to install big, high power heavy ion sources?

H. BLOSSER: The smallest first turn geometry in the K500 is approximately like the K50 first turn – the K500 orbit is about 30% smaller. This comfortably clears a source of the type we now use, and our intensity estimates are based on currents from this source. There is also room for a high power source of the GSI type.

0018-9499/79/0400-2047$00.75 ©1979 IEEE